Chapter 7
Stochastic Optimal Control of Wind-Resistant Structures with Viscous Dampers

7.1 Preliminary Remarks

The high-rise buildings experience alongwind-induced motions or acrosswind-induced motions when they are subjected to wind actions. The occupants would feel uncomfortable if these motions reach a certain amplitude. The structural performance, in this case, is generally denoted by the habitability, which is often measured by the wind-induced acceleration of structures (Chan and Chui 2006). The serviceability design problem of high-rise buildings associated with habitability enhancement is one of the most concerned issues, especially during typhoon seasons. The reports relevant to typhoon events in the past years often mentioned that the strong vibration of high-rise buildings results in discomfort or even dazzling state to occupants. Numerical investigations of TMD deployed in the building "Taipei 101" indicated that the vibration of the structure subjected to frequently occurring wind actions with a half-year return period would exceed 30% of the design maximum acceleration if removing the control device (Chung et al. 2013). Therefore, the serviceability-based control and design retain a practical significance to the high-rise buildings.

The structural control for mitigating wind-induced vibration can be largely categorized into the passive and active modalities. The former is a widely applied means due to its practical feasibility (Housner et al. 1997). A most efficient measure for mitigating the wind-induced vibration of structures is the damping reinforcement. The viscous dampers are proved to be an effective proposal of implementing the damping reinforcement owing to their many technical advantages (Housner et al. 1997; Patil and Jangid 2011), e.g., being insensitive to the working temperature (with steady behaviors from −40 centidegrees to 70 centidegrees) (Symans and Contantinou 1998), remaining a visco-response in a wide frequency domain (Soong and Constantinou 1994), exhibiting a damper force out of phase with displacement (Soong and Dargush 1997), and providing considerable damper force even in case of low structural velocity. Another highlighting feature of the viscous damper is its benefit

Y. Peng and J. Li, *Stochastic Optimal Control of Structures*,
https://doi.org/10.1007/978-981-13-6764-9_7

in acceleration control owing to a less stiffness and a larger damping that the damper supplies. Therefore, the viscous damper has been proved to the best control device for the wind-induced comfortability control of high-rise and ultra high-rise buildings. The parameter definition and placement optimization of viscous dampers are the critical issues associated with the stochastic optimal control of wind-induced structural comfortability. However, the viscous damper is a velocity-relevant damper, and exhibits a strong nonlinearity. The structure deployed with viscous dampers becomes a nonlinear system in essence. The primary task for the stochastic optimal control of viscously damped structures is thus seeking for a solving procedure with sufficient efficiency and accuracy.

In the present chapter, the equivalent linearization techniques with respect to the structural system attached with nonlinear viscous dampers are addressed first. The probabilistic criteria and numerical methods for the optimal design of viscous dampers used in randomly wind-induced vibration control of structures are provided. For validating purposes, the optimal control of wind-induced comfortability of a high-rising building is investigated, of which the randomness inherent in wind excitations is included.

7.2 Equivalent Linearization of Viscously Damped Systems

The stochastic optimal control of viscously damped structural systems involves the design of damper parameters and the optimization of damper deployments. This features practical significance for the high-rise building with available limited space. As mentioned in Chap. 1, the optimization methods for damper deployments can be categorized into three classes, i.e., the sequential method (Zhang and Soong 1992), the gradient method (Takewaki 1997; Peng et al. 2013), and the genetic algorithm based method (Singh and Moreschi 2002). These three classes of optimization methods all involve the iterative solution of viscously damped structures with nonlinearity. For this reason, a highly efficient method which allows for solving the viscously damped structures underlies the optimization and design of the viscous dampers.

The analysis methods for the damper control of structural wind-induced vibration are mainly classified into frequency-domain and time-domain methods. The frequency-domain method is widely used in practice due to the simple algorithm and the rigorous principle (Davenport 1961). The time-domain method can accurately secure the response details of structures even with nonlinear behaviors, which has been paid extensive attention in recent years. As to the reliability-based control for wind-induced vibration mitigation of structures, the time-domain method is usually required. It is revealed in previous investigations (Chen et al. 2017) that the equation of motion of viscously damped structural systems with low-velocity exponent dampers often refers to stiff problem, which belongs to a family of strong nonlinearities. This issue results in that the traditional equivalent linearization techniques such as the energy-dissipation equivalent linearization method and statistical linearization technique remain a challenge.

7.2.1 *Stiff Differential Equation for Viscously Damped Systems*

Consider a single-degree-of-freedom (SDOF) structural system attached with a viscous damper, the equation of motion of the controlled structure subjected to time-varying load $F(t)$ is given by

$$m\ddot{x}(t) + c\dot{x}(t) + kx(t) - F_D(\dot{x}(t)) = F(t) \tag{7.2.1}$$

where m, c, and k denote the mass, damping, and stiffness of the structure, respectively; $x(t)$, $\dot{x}(t)$ and $\ddot{x}(t)$ denote the displacement, velocity, and acceleration of the structure, respectively, which exhibit an opposing displacement and velocity as the piston; $F(t)$ denotes the external excitation; $F_D(\cdot)$ denotes the damper force exerted by the viscous damper:

$$F_D(\dot{x}(t)) = -c_D \text{sgn}(\dot{x}(t))|\dot{x}(t)|^{\alpha} \tag{7.2.2}$$

where c_D denotes the damping coefficient; α denotes the velocity exponent, which is a positive quantity between 0 and 1, being closer to 0 implying stronger nonlinearity. The velocity exponent is usually valued in the range $0.3 \leq \alpha \leq 0.5$ for the case of building control, and is usually valued in the range $0.15 \leq \alpha \leq 0.3$ for the case of bridge control. The sign $\text{sgn}(\cdot)$ is the signum function, taking value 1 for positive argument, -1 for negative argument, and otherwise 0.

The damper force of the viscous damper represented by Eq. (7.2.2) for different α and the same unit of damping coefficient $c_D = 1.0$ is shown in Fig. 7.1, in which the loaded sine wave of displacement exhibits unit amplitude and unit circular frequency. It is seen clearly that in the case $\alpha = 1.0$, it reduces to a linear damping; whereas in the case $\alpha = 0.0$, it becomes a dry-friction force. When $0 < \alpha < 1.0$,

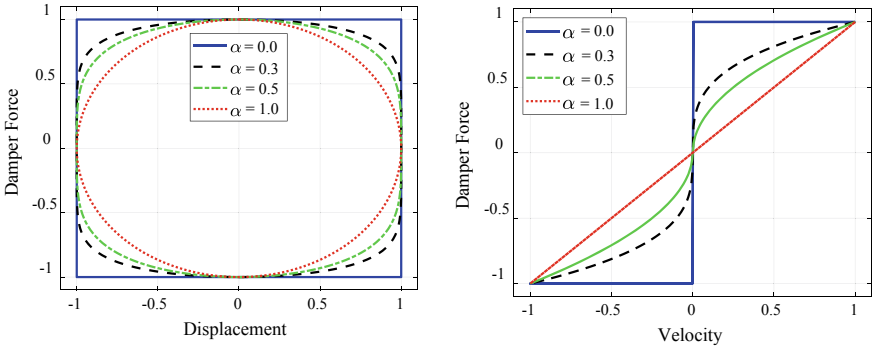

(a) damper force vs. dispalcement (b) damper force vs. velocity

Fig. 7.1 Damper force of viscous damper in cases of different velocity exponents

the smaller of the velocity exponent α, the stronger of nonlinearity that the viscous damper exhibits. Moreover, the hysteretic curve of the damper involves from the elliptical shape to the rectangular shape as the velocity exponent decreases. In the case of same maximum damper force and same maximum displacement, the smaller of the velocity exponent, the more similar to a rectangular shape with a larger area that the hysteretic curve gives rise to, which indicates a stronger energy-dissipation capacity of the viscous damper and a better control effectiveness on the viscously damped structure. However, the change of the damper force as the velocity arises to fast-varying and slow-varying behaviors. For instance, the damper force varies very fast in the case of low velocity close to zero if the velocity exponent $\alpha = 0.3$; while it varies mildly in other velocity domains. Such coexistence of fast-varying and low-varying behaviors of viscous dampers leads to a typical stiff system of the controlled structure attached with viscous damper. A stiff system can be revealed by its stiff differential equation.

To further clarify this problem, consider the case of free vibration, i.e., $F(t) = 0$ in Eq. (7.2.1). Substituting Eq. (7.2.2) into Eq. (7.2.1), and letting $y_1(t) = x(t)$, $y_2(t) = \dot{x}(t)$ lead to the state equation as follows:

$$\begin{cases} \dot{y}_1(t) = y_2(t) \\ \dot{y}_2(t) = -\frac{c}{m} y_2(t) - \frac{k}{m} y_1(t) - \frac{c_D}{m} \mathrm{sgn}(y_2(t)) |y_2(t)|^\alpha \end{cases} \tag{7.2.3}$$

In a vector form

$$\dot{\mathbf{Y}} = \mathbf{A}(\mathbf{Y}, t) \tag{7.2.4}$$

where

$$\begin{aligned} &\mathbf{Y} = (y_1(t), y_2(t))^{\mathrm{T}} \mathbf{A} = (A_1, A_2)^{\mathrm{T}} A_1(y_1(t), y_2(t)) = y_2(t) \\ &A_2(y_1(t), y_2(t)) = -\frac{c}{m} y_2(t) - \frac{k}{m} y_1(t) - \frac{c_D}{m} \mathrm{sgn}(y_2(t)) |y_2(t)|^\alpha \end{aligned} \tag{7.2.5}$$

The Jacobian matrix for Eq. (7.2.5) can thus be obtained by

$$\mathbf{J} = \begin{bmatrix} \frac{\partial A_1}{\partial y_1} & \frac{\partial A_1}{\partial y_2} \\ \frac{\partial A_2}{\partial y_1} & \frac{\partial A_2}{\partial y_2} \end{bmatrix} = \begin{bmatrix} 0 & 1 \\ -\frac{k}{m} & \left(-\frac{c}{m} - \alpha \frac{c_D}{m} |y_2(t)|^{\alpha - 1}\right) \end{bmatrix} \tag{7.2.6}$$

The characteristic equation can be obtained as

$$\lambda^2 + \left(\frac{c}{m} + \alpha \frac{c_D}{m} |\dot{x}(t)|^{\alpha - 1}\right) \lambda + \frac{k}{m} = 0 \tag{7.2.7}$$

where λ denotes the eigenvalues of the Jacobian matrix. If Eq. (7.2.7) satisfies the conditions as follows:

$$\begin{cases} \mathrm{Re}(\lambda_j) < 0, \quad j = 1, 2, \cdots, m \\ s := \max\limits_{1 \le j \le m} \left|\mathrm{Re}(\lambda_j)\right| / \min\limits_{1 \le j \le m} \left|\mathrm{Re}(\lambda_j)\right| \gg 1 \end{cases} \tag{7.2.8}$$

where $\mathrm{Re}(\cdot)$ denotes the real counterpart of the complex eigenvalues. Equation (7.2.1) is then defined as a stiff differential equation, where s denotes the stiff ratio.

For illustrative purposes, consider Eq. (7.2.1) as the first modal equation of a high-rise building structure, where the modal mass $m = 3.75 \times 10^7$ kg, the modal damping ratio $\zeta = 0.01$, and the fundamental period $T_n = 4.94$ s. Since the stiffness $k = \frac{4\pi^2 m}{T_n^2}$ and the damping coefficient $c = \frac{4\pi\zeta m}{T_n}$, Eq. (7.2.7) becomes

$$\lambda^2 + \left(\frac{4\pi\zeta}{T_n} + \alpha \frac{c_D}{m} |\dot{x}|^{\alpha-1}\right)\lambda + \frac{4\pi^2}{T_n^2} = 0 \tag{7.2.9}$$

The two roots of Eq. (7.2.9) are given by

$$\lambda_{1,2} = -\frac{1}{2}\left(\frac{4\pi\zeta}{T_n} + \alpha \frac{c_D}{m} |\dot{u}|^{\alpha-1}\right) \pm \frac{1}{2}\sqrt{\left(\frac{4\pi\zeta}{T_n} + \alpha \frac{c_D}{m} |\dot{u}|^{\alpha-1}\right)^2 - \frac{16\pi^2}{T_n^2}} \tag{7.2.10}$$

For notation convenience, let $\frac{4\pi\tilde{\zeta}_D}{T_n} = \alpha \frac{c_D}{m} |\dot{x}|^{\alpha-1}$, such that

$$\tilde{\zeta}_D = \alpha \frac{c_D T_n}{4\pi m} |\dot{x}|^{\alpha-1} \tag{7.2.11}$$

It is indicated that the argument defined in Eq. (7.2.11) is an instantaneous damping ratio due to its relevance with velocity. Then

$$\lambda_{1,2} = -\frac{2\pi}{T_n}\left(\zeta_t \pm \sqrt{\zeta_t^2 - 1}\right) \tag{7.2.12}$$

where $\zeta_t = \zeta + \tilde{\zeta}_D$, which could be noted as the instantaneous total damping ratio.

The following special cases are of interest for addressing the stiff ratio:

Case 1: If $c_D \equiv 0$, i.e., there is no viscous dampers in the system, then $\tilde{\zeta}_D \equiv 0$, and the two roots in Eq. (7.2.12) are thus reduced to $\lambda_{1,2} = -\frac{2\pi}{T_n}\left(\zeta \pm \sqrt{\zeta^2 - 1}\right)$. The damping ratio of the structure itself is usually far less than 1.0. For instance, it is usually less than 5% for concrete structures and in the range of 1%–3% for steel structures. The two roots are thus conjugate complex numbers $\lambda_{1,2} = -\frac{2\pi}{T_n}\left(\zeta \pm \mathrm{i}\sqrt{1 - \zeta^2}\right)$, where $\mathrm{i} = \sqrt{-1}$ denotes the imaginary unit. In this case, the stiff ratio $s = |\mathrm{Re}(\lambda_1)| / |\mathrm{Re}(\lambda_2)| = 1$.

Case 2: If $\alpha = 1$, i.e., the viscous damper is reduced to a linear damper, there is $\tilde{\zeta}_D = \frac{c_D T_n}{4\pi m}$. Generally, in engineering practice the additional "equivalent" damping ratio $\tilde{\zeta}_D$ owing to the installation of damping devices might be in the range of 2%–4%, and thus the total damping ratio of the controlled structure might be in the range of

4%–7%, which is still much smaller than 1.0. In this case, the two roots in Eq. (7.2.12) are conjugate complex numbers, and the stiff ratio is 1 as well.

Case 3: As the damping coefficient c_D increases and the other quantities keep fixed, the instantaneous damping ratio $\tilde{\zeta}_D$ will increase according to Eq. (7.2.11). When c_D is large enough, $\zeta_t^2 - 1 \geq 0$ will occur, i.e., the system becomes an instantaneous over-damped system. In this case, the stiff ratio $s = \frac{\mathrm{Re}(\lambda_1)}{\mathrm{Re}(\lambda_2)} = \frac{\zeta_t + \sqrt{\zeta_t^2 - 1}}{\zeta_t - \sqrt{\zeta_t^2 - 1}} = \left(\zeta_t + \sqrt{\zeta_t^2 - 1}\right)^2$, which tends to $s \approx 4\zeta_t^2$, and the stiff ratio will increase very fast against the instantaneous total damping ratio, and in turn against the increase of c_D.

Case 4: As the fundamental period T_n increases when the other quantities are kept fixed, the instantaneous damping ratio $\tilde{\zeta}_D$ will increase. When T_n is large enough, $\zeta_t^2 - 1 \geq 0$ might occur. Similar to Case 3, the stiff ratio will be given also by $s = \left(\zeta_t + \sqrt{\zeta_t^2 - 1}\right)^2$. Thus, in this case, the stiff ratio will increase very fast against the instantaneous total damping ratio, and in turn against the increase of T_n. Generally, high-rise buildings have longer fundamental periods. Therefore, the stiff ratio of high-rise building structures might be large. This is just the case that the wind-induced vibration of high-rise buildings shall be suppressed by the control systems consisting of viscous dampers.

Case 5: As the velocity exponent α decreases and the other quantities are fixed, the instantaneous damping ratio $\tilde{\zeta}_D$ will first increase and then decrease from some "turning point". The derivative of $\tilde{\zeta}_D$ with respect to α is given by $\frac{\partial \tilde{\zeta}_D}{\partial \alpha} = \frac{c_D T_n}{4\pi m} |\dot{x}|^{\alpha - 1} [1 + \alpha \ln(|\dot{x}|)]$, and thus the "turning point" will occur when $\frac{\partial \tilde{\zeta}_D}{\partial \alpha} = 0$, i.e., $\alpha = -\frac{1}{\ln(|\dot{x}|)}$, which is related to the velocity. Therefore, with the decrease of α from one to zero, the stiff ratio s first equals 1 when $\zeta_t^2 - 1 \leq 0$, and then quadratically increase to its peak at the "turning point" following the same pattern as Case 3 and Case 4, afterward it decreases to 1 again in a sharp manner when $\alpha = 0$. One might recognize that the "turning point" is straightforwardly related to the velocity that the smaller the velocity is, the closer the "turning point" approaches to zero.

To reveal the influence parameters on the stiff ratio of the structural system intuitively, case studies are carried out. Since the damper force changes very fast in the case of a small velocity, the velocity is set as $\dot{x} = 0.1$ mm/s. Shown in Fig. 7.2 are the stiff ratios against different parameters of viscously damped structural systems, including the damping coefficient of viscous dampers, the fundamental period of the structural system, and the velocity exponent. It is observed that the stiff ratio quadratically increases by the order of magnitudes against the increase of damping coefficient and the fundamental period; see Fig. 7.2a. As the velocity exponent decreases from 1 down to 0, however, the stiff ratio first experiences a stage with value 1.0, then quadratic increase to the "turning point", and decreases sharply; see Fig. 7.2b. This result is in agreement with the discussions in Case 1–Case 5. One might recognize that a higher damping ratio indicates a larger damper force. Clearly, if the damping ratio is too small, the viscous damper has little effects on the response of the system, and it could be expected that the stiff ratio will also change slightly. Therefore, only

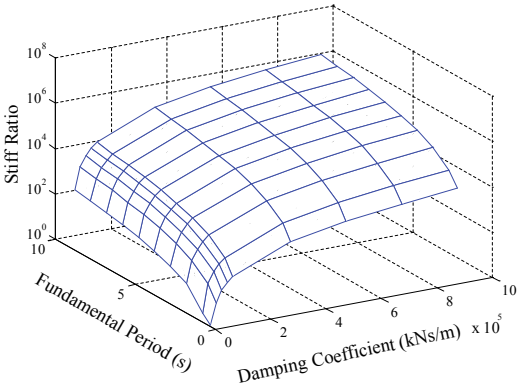

(a) stiff ratio vs. damping coefficient and fundamental period (velocity exponent $\alpha = 0.5$)

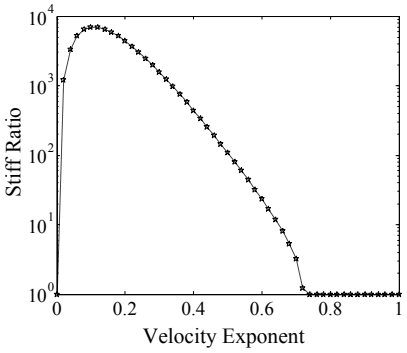

(b) stiff ratio vs. velocity exponent (damping coefficient $c_D = 10000\text{kN}\cdot(\text{s/m})^{\alpha}$, fundamental period $T_n = 4.94$ s)

Fig. 7.2 Stiff ratio against different parameters of viscously damped systems

for relatively large damping coefficient its effect on stiff ratio becomes significant. The stiff ratio being relatively large for longer fundamental period is also physically reasonable, since a longer fundamental period indicates a lower predominant frequency in the response. A higher frequency content might be compensated by the sharp change of the damper force of viscous dampers with a moderate velocity exponent α. This is extremely significant for high-rise buildings installed with viscous damper, owing to their fundamental periods are usually longer than 2 s even as high as nearly 10 s, and the damping component of viscous dampers is usually smaller than 0.5 down to 0.3.

Generally, a system is denoted by a stiff differential equation if its stiff ratio is greater than 10^p ($p \geqslant 1$). It is seen from Fig. 7.2 that high-rise buildings with the fundamental period longer than 2 s, attached with viscous dampers exhibiting the damping coefficient more than 10,000 kN(s/m)$^{\alpha}$ and the velocity exponent 0.3–0.5,

are seriously stiff since their stiff ratios are typically in the order of magnitude of 10^2 or higher.

7.2.2 Solution of Viscously Damped Systems

The equation of motion of an MDOF structure attached with viscous dampers can be denoted by

$$\mathbf{M}\ddot{\mathbf{X}}(t) + \mathbf{C}\dot{\mathbf{X}}(t) + \mathbf{K}\mathbf{X}(t) + \mathbf{F}_D(\dot{\mathbf{X}}(t)) = \mathbf{F}(\boldsymbol{\Theta}, t) \tag{7.2.13}$$

where $\mathbf{M}$, $\mathbf{C}$, and $\mathbf{K}$ are the mass, damping, and stiffness matrices, respectively; $\mathbf{X}$, $\dot{\mathbf{X}}$, and $\ddot{\mathbf{X}}$ are the structural displacement, velocity, and acceleration, respectively; $\mathbf{F}(\boldsymbol{\Theta}, t)$ denotes the random wind load; $\boldsymbol{\Theta}$ is the random vector denoting the randomness inherent in the random wind load; $\mathbf{F}_D(\dot{\mathbf{X}}(t))$ denotes the attached damper force:

$$\mathbf{F}_D(\dot{\mathbf{X}}(t)) = \mathbf{S} \cdot \left(\left|\mathbf{T}_{\dot{\mathbf{X}}}\right|^{\alpha} \times \operatorname{sgn}\left(\mathbf{T}_{\dot{\mathbf{X}}}\right)\right) = \begin{bmatrix} c_{D,1} & -c_{D,2} & 0 & \cdots & 0 & 0 \\ 0 & c_{D,2} & -c_{D,2} & \cdots & 0 & 0 \\ 0 & 0 & c_{D,3} & \cdots & 0 & 0 \\ \vdots & \vdots & \vdots & \vdots & \vdots & \vdots \\ 0 & 0 & 0 & \cdots & c_{D,n-1} & -c_{D,n} \\ 0 & 0 & 0 & \cdots & 0 & c_{D,n} \end{bmatrix}$$
$$\cdot \left(\left| \begin{bmatrix} 1 & 0 & 0 & \cdots & 0 & 0 \\ -1 & 1 & 0 & \cdots & 0 & 0 \\ 0 & -1 & 1 & \cdots & 0 & 0 \\ \vdots & \vdots & \vdots & \vdots & \vdots & \vdots \\ 0 & 0 & 0 & \cdots & 1 & 0 \\ 0 & 0 & 0 & \cdots & -1 & 1 \end{bmatrix} \begin{Bmatrix} \dot{X}_1 \\ \dot{X}_2 \\ \dot{X}_3 \\ \vdots \\ \dot{X}_{n-1} \\ \dot{X}_n \end{Bmatrix} \right|^{\alpha} \times \operatorname{sgn} \left(\begin{bmatrix} 1 & 0 & 0 & \cdots & 0 & 0 \\ -1 & 1 & 0 & \cdots & 0 & 0 \\ 0 & -1 & 1 & \cdots & 0 & 0 \\ \vdots & \vdots & \vdots & & \vdots & \vdots \\ 0 & 0 & 0 & \cdots & 1 & 0 \\ 0 & 0 & 0 & \cdots & -1 & 1 \end{bmatrix} \begin{Bmatrix} \dot{X}_1 \\ \dot{X}_2 \\ \dot{X}_3 \\ \vdots \\ \dot{X}_{n-1} \\ \dot{X}_n \end{Bmatrix} \right) \right) \tag{7.2.14}$$

where $\mathbf{S}$ denotes the damping coefficient matrix; $c_{D,j}$ denotes the total damping coefficient of the jth interstory with viscous damper; $\mathbf{T}_{\dot{\mathbf{X}}}$ denotes the interstory velocity vector, and $\left|\mathbf{T}_{\dot{\mathbf{X}}}\right|^{\alpha}$ indicates taking the component-wise power, i.e., $\left|\mathbf{T}_{\dot{\mathbf{X}}}\right|^{\alpha} = \left(\left|T_{\dot{X},1}\right|^{\alpha}, \left|T_{\dot{X},2}\right|^{\alpha}, \cdots, \left|T_{\dot{X},n}\right|^{\alpha}\right)^{\mathrm{T}}$, where $T_{\dot{X},j}$ denotes the jth component of the vector $\mathbf{T}_{\dot{\mathbf{X}}}$.

It is found quite often that the equation of motion of a high-rise building installed with nonlinear viscous dampers is surprisingly difficult to solve by conventional numerical schemes, just due to its stiff problem as addressed previously. Most of the widely used time integral schemes, such as the Newmark method and the Wilson method, suffer from instability or spurious numerical spikes. In fact, as to solving ordinary differential equations, a family of backward differentiation formulae

(BDF) is demonstrated to be efficient. The extended formulation of BDF is written as (Shampine and Reichelt 1997)

$$\sum_{j=1}^{k} \frac{1}{j} \nabla^j z_{n+1} = hL(t_{n+1}, z_{n+1}) + \kappa \gamma_k \left(z_{n+1} - z_{n+1}^{(0)} \right) \tag{7.2.15}$$

where

$$\gamma_k = \sum_{j=1}^{k} \frac{1}{j}, \quad z_{n+1} - z_{n+1}^{(0)} = \nabla^{k+1} z_{n+1} \tag{7.2.16}$$

in which $\nabla^j z_n = \nabla^{j-1} z_n - \nabla^{j-1} z_{n-1}$ denotes the operator of backward differentiation, $\nabla^0 z_n = z_n$; z_n denotes the system state; k denotes the computational order; h denotes the step-length of differentiation; L denotes the system operator of initial value problems, i.e. $\dot{z} = L(t, z),\ z(t_0) = z_0$; κ is a scalar parameter. Equation (7.2.15) reduces to the standard BDF in the case $\kappa = 0$.

It is seen from Eq. (7.2.15) that although the backward differentiation formulae for solving the nonlinear systems are accurate, their solutions involve multiple-step schemes and are not suitable for the iterative optimization and design of viscously damped structural systems. In practice, the equivalent linearization techniques are usually employed which transfers the original nonlinear system into a linearized system as a certain equivalent criterion resulting in the responses between original nonlinear and linearized systems to be the same or in an acceptable error range. Among those equivalent linearization techniques, the widely used is the energy-dissipation equivalent linearization method.

The equivalent criterion of the energy-dissipation equivalent linearization method is that the energy dissipations of attached viscous dampers to the equivalent linearized system and to the original nonlinear system are equal. The additional equivalent damping ratio as the energy-dissipation equivalent criterion $\zeta_k^{(\text{E-E})}$ is given by (Seleemah and Costantinou 1997):

$$\zeta_k^{(\text{E-E})} = \frac{T_k^{2-\alpha} \sum_j c_{D,j} \lambda \left[(u_{k,j} - u_{k,j-1}) \cos(\theta_j) \right]^{1+\alpha}}{(2\pi)^{3-\alpha} A_k^{1-\alpha} \sum_i m_i u_{k,i}^2} \tag{7.2.17}$$

where

$$\lambda = 2^{2+\alpha} \frac{\Gamma^2(1 + \alpha/2)}{\Gamma(2 + \alpha)} \tag{7.2.18}$$

where T_k denotes the period of the kth vibrational mode; θ_j denotes the angle between the story and viscous damper in the jth interstory; $u_{k,j}$ denotes the modal displacement the jth story of the kth vibrational mode; m_i denotes the mass of the jth story;

A_k denotes the roof displacement amplitude of the kth vibrational mode in unit of modal displacement $u_{k,j}$; $\Gamma(\cdot)$ denotes the Gamma function $\Gamma(z) = \int_0^\infty t^{z-1} \big/ \mathrm{e}^t \mathrm{d}t$.

It is seen that the formulation of the equivalent damping ratio $\zeta_k^{(\mathrm{E\text{-}E})}$ includes the roof displacement amplitude of the kth vibrational mode A_k, indicating that the solution of equivalent damping ratio needs a known roof displacement amplitude. However, solving the roof displacement amplitude needs to have the equivalent damping ratio in advance. Therefore, the energy-dissipation equivalent linearization method involves an iterative scheme.

It is noted that in the energy-dissipation equivalent linearization method, the structural response is assumed to be a harmonic process, which is inconsistent with the response characteristics of engineering structures subjected to dynamic excitations such as seismic ground motion and wind load. Another route to solve the nonlinear system is the stochastic equivalent linearization method, i.e., the statistical linearization technique (Roberts and Spanos 1990). In the statistical linearization technique, the structural response is assumed to be a Gaussian stationary process, and the difference between the linearized system and original nonlinear system is minimized in the sense of mean square.

By virtue of the statistical linearization technique, the equivalent damping ratio of a viscously damped structural system can be denoted by (see Appendix D)

$$\zeta_k^{(\mathrm{S\text{-}E})} = \eta_k \rho(\alpha) \left(\frac{G_{\tilde{F}_k(t)}(\omega)}{\left(\zeta_k^{(\mathrm{S\text{-}E})} + \zeta_k\right)\omega_k} \right)^{(\alpha-1)/2} \tag{7.2.19}$$

where $\rho(\alpha) = \Gamma\big(1+\alpha/2\big)\sqrt{2^{3-\alpha}\pi^{\alpha-2}}$; $G_{\tilde{F}_k(t)}(\omega)$ denotes the one-sided power spectral density of the generalized excitation $\tilde{F}_k(t) = \phi_k^{\mathrm{T}}\mathbf{F}(\boldsymbol{\Theta}, t) \big/ \big(\phi_k^{\mathrm{T}}\mathbf{M}\phi_k\big)$ of the kth vibrational mode; $\eta_k = q_k \big/ (2\bar{m}_k\omega_k)$, $q_k = \sum\limits_{j=1}^{n} \Big(c_{D,j}\Delta_j^{(k)} + c_{D,j+1}\Delta_{j+1}^{(k)}\Big)u_{k,j}^2 - 2\sum\limits_{j=2}^{n} c_{D,j}\Delta_j^{(k)}u_{k,j}u_{k,j-1}$, $\Delta_j^{(k)} = \left|u_{k,j} - u_{k,j-1}\right|^{\alpha-1}$; $\bar{m}_k$ denotes the modal mass of the kth vibrational mode; ζ_k, ω_k denote the damping ratio and the circular frequency of the kth vibrational mode, respectively.

To verify the effectiveness and accuracy of equivalent linearization techniques and the BDF, a 20-story shear frame controlled by viscous dampers is investigated. The basic information of the structure is as follows: the structural height is 72 m with story height of 3.6 m and depth–width ratio of 2.2; the mass of each story is $m_1 = m_2 = \cdots = m_{20} = 2.0 \times 10^5$ kg, and the interstory stiffness is $k_1 = \cdots = k_4 = 1.7 \times 10^5$ kN/m, $k_5 = \cdots = k_{10} = 1.5 \times 10^5$ kN/m, $k_{11} = \cdots = k_{16} = 1.2 \times 10^5$ kN/m, $k_{17} = \cdots = k_{20} = 1.0 \times 10^5$ kN/m. The damping ratios of the first two vibrational modes are both 0.01. The structural damping is represented by Rayleigh damping matrix $\mathbf{C} = a\mathbf{M} + b\mathbf{K}$. The circular frequencies of the first ten vibrational modes are 2.09, 5.88, 9.74, 13.45, 17.27, 20.94, 24.28, 27.81, 30.90, and 33.93 rad/s, receptively. The wind-induced vibration control of the structure is carried out using the viscous

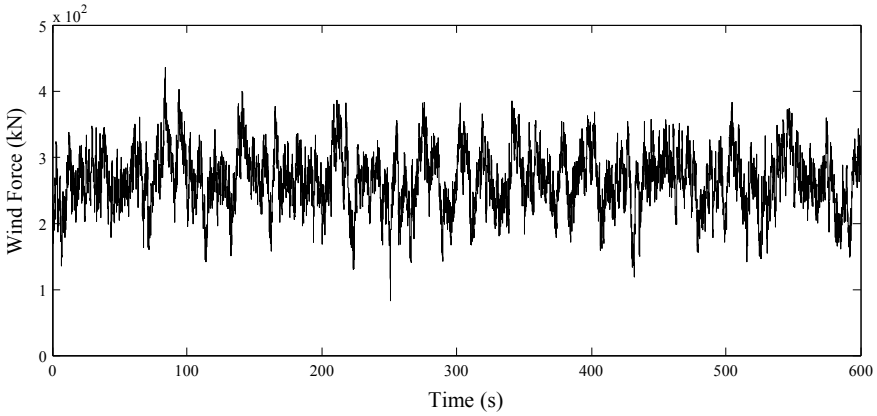

Fig. 7.3 Time history of representative wind force on the structural roof

dampers. For illustrative purposes, the viscous dampers are deployed uniformly in the interstories along the story level. The additional damping coefficient at each interstory is 500 kN(s/m)$^{\alpha}$, where the velocity exponent is valued by $\alpha = 1.0, 0.5, 0.3$.

The Newmark-β scheme on the linearized system by the energy-dissipation equivalent linearization method (EEN), the Newmark-β scheme on the linearized system by the stochastic equivalent linearization method (SEN), and the backward differentiation formulae on the original nonlinear system (BDF) are employed to carry out the time-domain analysis. The wind excitation is represented by the spatial fluctuating wind-velocity field model addressed in Sect. 2.5.2. The three basic random parameters included in the wind velocity Fourier spectrum model are valued as: the 10-min mean wind velocity $\bar{U}_{10}$ at the standard height 10 m is assumed to follow the extreme-value type I distribution with mean 39.33 m/s and coefficient of variation 0.1; the surface roughness length z_0 is assumed to follow the log-normal distribution with mean 0.2 m and coefficient of variation 0.2; the zero-phase evolution time T_e is assumed to follow the Gamma distribution with mean 0.902×10^9 s and coefficient of variation 0.1. A representative time history of the random wind excitation on the structural roof is shown in Fig. 7.3. The approaching flow is assumed to be perpendicular to the building surface. Under the representative wind excitation, the roof displacement and roof acceleration of the viscously damped structure with variant velocity exponents and using different numerical schemes are shown in Figs. 7.4, 7.5, 7.6.

It is seen that the structural responses by the three schemes match well with each other in the case of velocity exponent 1.0. With the decreasing of velocity exponent, the result of the energy-dissipation equivalent linearization method deviates with that of the BDF to a larger extent, in comparison with the stochastic equivalent linearization method. In the case of velocity exponent 0.3, this tendency becomes much more significant, that is, the result of the stochastic equivalent linearization method is much closer to the BDF, in comparison with the energy-dissipation equivalent

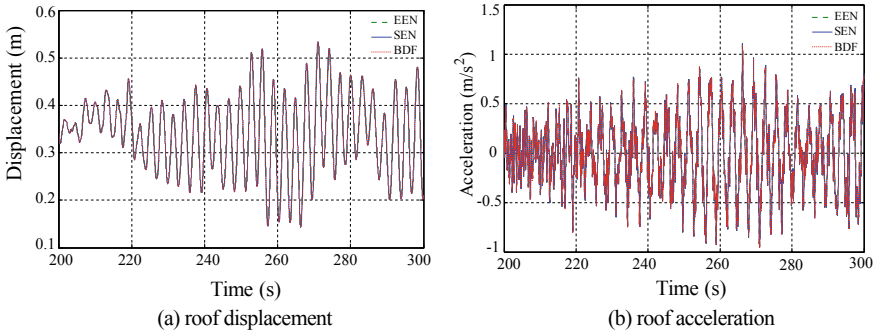

(a) roof displacement (b) roof acceleration

Fig. 7.4 Comparison of roof responses using different schemes in the case of velocity exponent 1.0

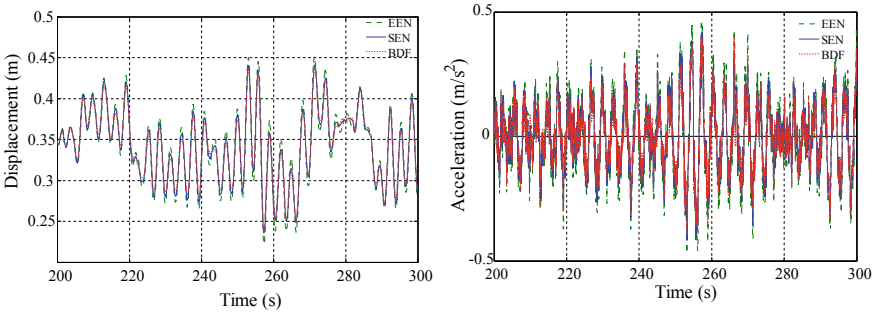

(a) roof displacement (b) roof acceleration

Fig. 7.5 Comparison of roof responses using different schemes in the case of velocity exponent 0.5

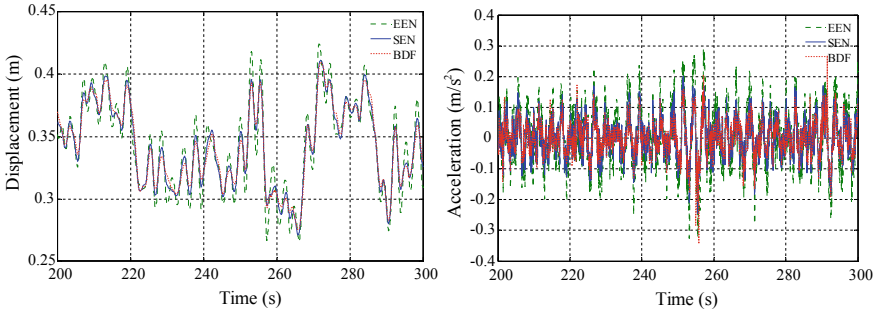

(a) roof dispalcement (b) roof acceleration

Fig. 7.6 Comparison of roof responses using different schemes in the case of velocity exponent 0.3

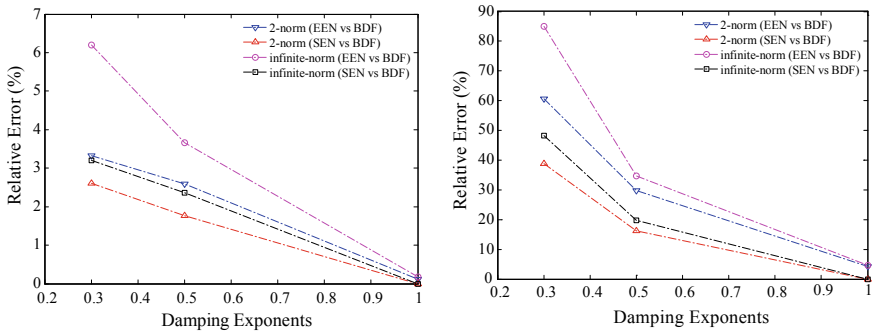

Fig. 7.7 Relative errors in 2-norm and infinite-norm of roof responses with different velocity exponents and using different schemes

linearization method. It is thus demonstrated that the stochastic equivalent linearization method has a considerable accuracy even when the nonlinearity of the viscously damped structural system is relatively strong, and the energy-dissipation equivalent linearization method is shown to be conservative.

The relative errors in 2-norm and infinite-norm of roof responses with different velocity exponents using the measure of relative error in 2-norm using the three schemes "EEN" and "SEN" compared to the "BDF" are shown in Fig. 7.7. It is well recognized that it is smaller than that in infinite-norm both in terms of the roof displacement and roof acceleration; the relative errors of acceleration are more than those of displacement by over 10 times, indicating a computational challenge inherent in the accurate solution of the structural acceleration. It is also seen that the relative error would increase rapidly with the reduction of velocity exponent. Meanwhile, the relative errors of structural responses between the energy-dissipation equivalent linearization method and the BDF are always larger than those between the stochastic equivalent linearization method and the BDF, no matter in 2-norm or in infinite-norm.

In summary, the stochastic equivalent linearization method is an elegant scheme since it reveals the stochastic essence of structural responses to some extent by invoking the Gaussian-process assumption of structural responses, and gains the equivalent modal damping ratio through minimizing the mean-square error between the linearized system and the original nonlinear system. In comparison with the energy-dissipation equivalent linearization method, the stochastic equivalent linearization method attains a more accurate solution that is more close to the result of the BDF. A solution with considerable accuracy and efficiency can thus be obtained by performing frequency-domain and time-domain analysis upon the linearized structural system, especially upon the high-rise buildings structures, where intermediate nonlinear dampers are the most common ones to be installed for performance enhancement. The stochastic equivalent linearization method is thus used to facilitate the serviceability-based optimal design of viscously damped structures as both the cri-

teria of minimizing the standard deviation and of minimizing the exceedance probability of roof acceleration.

7.3 Optimal Deployment of Viscous Dampers

As mentioned in Sect. 5.3, the comfortability is one of the critical arguments representing the performance of structural systems, which is usually measured by the acceleration. As to the high-rise buildings, the roof acceleration is generally far larger than other stories. In practice, the roof acceleration control is thus an efficient means for enhancing the structural comfortability.

Since the structural responses under the random excitations are random processes, the probabilistic criteria similar to the proposal in Chap. 4 can be employed in the present investigation. The probabilistic criterion of the conventional serviceability design is usually defined as the standard deviation or the peak value of wind-induced roof acceleration of structures (Huang et al. 2011). Considering the fundamental value of reliability in the optimization and design of structural performance, two families of serviceability criteria are thus employed with the minimization of single-objective performance function as follows:

(i) serviceability criterion 1 (SC-1): minimizing the standard deviation of roof acceleration.

$$c_{D,i}^{*} = \arg\min_{c_{D,i}}\{J_2\} = \arg\min_{c_{D,i}}\left\{\sigma_{\ddot{X}_n}\Big|\left\{\sum_i c_{D,i} = C_{D,\text{total}}\right\}\right\}, \quad i = 1, 2, \ldots, n \tag{7.3.1}$$

where $\sigma_{\ddot{X}_n}$ denotes the standard deviation of roof acceleration; $c_{D,i}^{*}$ denotes the optimal damping coefficient of the viscous dampers allocated in the ith interstory; $C_{D,\text{total}}$ denotes the target of total cost in terms of the sum of damping coefficient of the viscous dampers allocated in all the structural interstories. It is thus initiated that using the serviceability criterion shown in Eq. (7.3.1), the optimal distribution of damping coefficients related to the damper sizes and placements can be attained.

(ii) serviceability criterion 2 (SC-2): minimizing the exceedance probability of roof acceleration

$$\begin{aligned} c_{D,i}^{*} &= \arg\min_{c_{D,i}}\{J_2\} \\ &= \arg\min_{c_{D,i}}\left\{\Pr\left\{\bigcup_{t\in[0,T]}\left(\left|\ddot{X}_n(t)\right| > \ddot{X}_{\text{thd}}\right)\right\}\Big|\left\{\sum_i c_{D,i} = C_{D,\text{total}}\right\}\right\}, \\ & i = 1, 2, \ldots, n \end{aligned} \tag{7.3.2}$$

where $\ddot{X}_n(t)$ denotes the roof acceleration in the time interval $[0, T]$; $\ddot{X}_{\text{thd}}$ denotes threshold of the roof acceleration; $\Pr\{\cdot\}$ denotes the probability of random event. It is indicated that by virtue of the generalized optimal control policy, the serviceability criterion shown in Eq. (7.3.2) can accommodate the optimal design of damper parameters and placement so as to guarantee sufficient structural comfortability. One might recognize that this serviceability criterion is constructed according to the first-passage problem, of which the exceedance probability of roof acceleration can be readily solved via the generalized probability density evolution equations and the equivalent extreme-value event criterion.

The stochastic equivalent linearization method has been proved to exhibit high efficiency and accuracy for solving nonlinear multi-degree-of-freedom systems, which is thus first applied to carry out the linearization of nonlinear structural systems attached with viscous dampers. As to the linearized system, the modal superposition method in frequency-domain and the probability density evolution method with time-domain analysis by Newmark-β schemes are employed to solve the performance function J_2 in the serviceability criteria shown in Eqs. (7.3.1) and (7.3.2), respectively.

By virtue of the statistical linearization technique shown in Eq. (7.2.19), the additional equivalent damping ratio of viscously damped structures can be gained, and the nonlinear structural system is readily transferred into a linearized structural system. In modal space, the linearized system can be decomposed to a series of single-degree-of-freedom systems with independent equations of motion as follows:

$$\ddot{u}_j(t) + 2\zeta_j^{(\text{e})}\omega_j\dot{u}_j(t) + \omega_j^2 u_j(t) = \tilde{F}_j(t) \tag{7.3.3}$$

where $\tilde{F}_j(t) = \phi_j^{\text{T}}\mathbf{F}(\boldsymbol{\Theta}, t)\Big/\bar{m}_j$ denotes the generalized wind load of the jth vibrational mode; $\omega_j = \sqrt{\bar{k}_j\Big/\bar{m}_j}$ denotes the circular frequency of the jth vibrational mode; $\zeta_j^{(\text{e})} = \zeta_j^{(\text{S-E})} + \zeta_j$ denotes the sum of the inherent damping ratio and the equivalent damping ratio of the jth vibrational mode; $\bar{m}_j$, $\bar{k}_j$ denote the generalized mass and generalized stiffness of the jth vibrational mode, respectively; ϕ_j^{T} denotes the jth modal vector.

According to the modal superposition method, the cross-power spectral density of generalized wind load between modes i and j is represented by

$$S_{\tilde{F}_j\tilde{F}_k}(\omega) = \frac{1}{\bar{m}_j\bar{m}_k}\phi_j^{\text{T}}\mathbf{S}_{\mathbf{F}}(\omega)\phi_k \tag{7.3.4}$$

where $\mathbf{S}_{\mathbf{F}(t)}$ denotes the power spectral density matrix of wind load. The power spectral density of generalized structural responses $u_j(t)$ can be obtained by integrating the frequency response transfer function of systems and the power spectral density of generalized wind load:

$$S_{U_j}(\omega) = \left|H_j(\omega)\right|^2 S_{\tilde{F}_j}(\omega) \tag{7.3.5}$$

where $H_j(\omega)$ denotes the frequency response transfer function:

$$\left|H_j(\omega)\right|^2 = \frac{1}{\left(\omega_j^4 - 2\omega_j^2\omega^2 + \omega^4\right) + 4\left[\zeta_j^{(e)}\right]^2\omega_j^2\omega^2} \tag{7.3.6}$$

The power spectral density of the ith story displacement then can be written as

$$S_{X_j}(\omega) = \sum_{k=1}^{n} \phi_{jk}^2 S_{U_j}(\omega) = \sum_{k=1}^{n} \phi_{jk}^2 \left|H_j(\omega)\right|^2 S_{\tilde{F}_j}(\omega) \tag{7.3.7}$$

where ϕ_{jk} denotes the kth component of the jth modal vector of structural systems.

According to the relation between the power spectral densities of the structural responses and their differentiated arguments, the power spectral densities of story acceleration and those of story displacement have the relation function as follows:

$$S_{\ddot{X}_j}(\omega) = \omega^4 S_{X_j}(\omega) \tag{7.3.8}$$

The mean-square roof acceleration of the structure is then given by

$$\sigma_{\ddot{X}_j}^2 = \int_{-\infty}^{\infty} \omega^4 S_{X_j}(\omega)\mathrm{d}\omega = \sum_{k=1}^{n} \phi_{jk}^2 \int_{-\infty}^{\infty} \omega^4 \left|H_j(\omega)\right|^2 S_{\tilde{F}_j}(\omega)\mathrm{d}\omega \tag{7.3.9}$$

According to the equivalent extreme-value event criterion, the extreme value of roof acceleration $\ddot{X}_n$ in the time interval $[0, T]$ is defined by

$$W(\boldsymbol{\Theta}, T) = \max_{t\in[0,T]}\left(\left|\ddot{X}_n(\boldsymbol{\Theta}, t)\right|\right) \tag{7.3.10}$$

Introducing a pseudo random process, there is

$$Z(\tau) = \varphi(W(\boldsymbol{\Theta}, T), \tau) \tag{7.3.11}$$

$$Z(\tau)|_{\tau=\tau_0} = 0,\ Z(\tau)|_{\tau=\tau_c} = W(\boldsymbol{\Theta}, T) \tag{7.3.12}$$

According to the probability preservation principle, the joint probability density function $p_{Z\boldsymbol{\Theta}}(z, \boldsymbol{\theta}, \tau)$ of $(Z(\tau), \boldsymbol{\Theta})$ satisfies the generalized probability density evolution equation as follows (Li and Chen 2009):

$$\frac{\partial p_{Z\boldsymbol{\Theta}}(z, \boldsymbol{\theta}, \tau)}{\partial \tau} + \dot{Z}(\tau)\frac{\partial p_{Z\boldsymbol{\Theta}}(z, \boldsymbol{\theta}, \tau)}{\partial z} = 0 \tag{7.3.13}$$

where τ denotes the generalized time. The associated initial condition is given by

$$p_{Z\boldsymbol{\Theta}}(z, \boldsymbol{\theta}, \tau_0) = \delta(z - z_0) p_{\boldsymbol{\Theta}}(\boldsymbol{\theta}) \tag{7.3.14}$$

The joint probability density function $p_{Z\boldsymbol{\Theta}}(z, \boldsymbol{\theta}, \tau)$ can be then obtained by solving Eq. (7.3.13), in view of the numerical procedure solving the generalized probability density evolution equation addressed in Sect. 2.3.3. The probability density function of extreme value of the roof acceleration $Z(\tau_c)$ is then obtained:

$$p_Z(z, \tau_c) = \int_{\Omega_{\boldsymbol{\Theta}}} p_{Z\boldsymbol{\Theta}}(z, \boldsymbol{\theta}, \tau_c) \mathrm{d}\boldsymbol{\theta} \tag{7.3.15}$$

where $\Omega_{\boldsymbol{\Theta}}$ is the distribution space of $\boldsymbol{\Theta}$.

The dynamic reliability of structures is then given by

$$R(T) = \Pr\{W(\boldsymbol{\Theta}, T) \in \Omega_s\} = \int_0^{\ddot{X}_{\text{thd}}} P_Z(z, \tau_c) \mathrm{d}z \tag{7.3.16}$$

where $P_Z(z, \tau_c)$ denotes probability density of the virtual random process $Z(\tau)$ at the instant of time $\tau = \tau_c$.

The failure probability of roof acceleration $\ddot{X}_n$ in the time interval $[0, T]$ is then given by

$$\Pr\left\{ \bigcup_{t \in [0,T]} \left(\left| \ddot{X}_n(t) \right| > \ddot{X}_{\text{thd}} \right) \right\} = 1 - \int_0^{\ddot{X}_{\text{thd}}} P_Z(z, \tau_c) \mathrm{d}z \tag{7.3.17}$$

As mentioned in Sect. 7.2, the optimization methods for the damper deployment include the case-sequential scheme, the minimum gradient scheme, and the genetic algorithm. The former two schemes are both explicit strategies aiming at approaching the performance objective, which provide feasibility for the decision maker who is able to readily define the optimal parameters and placements of the viscous dampers in steps according to the structural performance. In comparison with the case-sequential scheme, the minimum gradient method exhibits the capacity with more expeditious convergence (Peng et al. 2013). However, the genetic algorithm is an implicit strategy aiming at minimizing the objective function. Although a repeat optimization might be incurred once the structural performance objective changes and the constraint on the optimization needs to be redefined, the genetic algorithm still has been widely used in the optimization and design of viscous dampers due to its good adaptability and excellent global optimization capability (Silvestri and Trombetti 2007). As to the issue of wind-induced comfortability control of high-rise buildings, an updated scheme for gaining a higher convergence velocity is developed by integrating the genetic algorithm and the minimum gradient criterion where the standard deviation and exceedance probability of the roof acceleration at the searching points and their change rates, i.e., gradient, are included.

The genetic algorithm is an iterative procedure following the rule of fittest to survive. In each generation of the population, the individuals are first selected according to the evaluation results of the individual fitness values in the addressed problem. The individual with larger fitness value exhibits a larger possibility of being selected. Then the crossover and mutation similar to the genetic operator in the genetics are carried out to yield the next generation of the population. This process results in that the next generation has a stronger fitness in the problem domain. The individuals in the last generation can be viewed as the optimal solution to the problem. The genetic algorithm involves a three-step procedure, i.e., selection, crossover, and mutation. As to the problem of viscous damper deployment with respect to the minimization of exceedance probability of roof acceleration, the fitness evaluations of individuals in each generation of population all involves solving the generalized probability density evolution equations, which incurs an unacceptable computational cost. In order to reduce the calculation efforts, the neural network algorithm is utilized.

The neural network algorithm aims at building the nonlinear mapping model exhibiting memory and prediction capacities through the training and predicting on the provided data (Rojas 1996). Utilizing the nonlinear mapping model, the computational cost of the objective function is saved, and the computational efficiency can be enhanced significantly.

The support vector machine (SVM) is employed serving as the tool for modeling of the neural network. The SVM has a distinguished ability for efficient prediction of the objective function of individuals, which can significantly reduce the computational cost (Haykin 2007). The flowchart of the SVM-based genetic algorithm is shown in Fig. 7.8. It is seen that the individual fitness of genetic algorithm relies upon the SVM, which thus plays a critical role in enhancing the accuracy and efficiency of the optimization procedure.

7.4 Case Studies

As a practical application of the optimal design of viscous dampers in the wind-induced comfortability control of high-rise buildings, a 58-story steel structure subjected to random wind excitations is studied. The height of the structure is 249 m, and the building area is 1.25 km^2. According to the Chinese Code for Design Loads of Building Structures (GB50009-2012), the structural basic wind pressure is 0.75 kN/m^2, the occupant-comfortability validation wind pressure is 0.45 kN/m^2, and the ground surface roughness belongs to type A.

Using the software PKPM to carry out the finite-element modeling and the analysis, the structural wind-induced responses can be readily derived from the formulae shown in the Chinese Code for Steel Structure of High-Rise Buildings (JGJ99-1998) and in the Chinese Code for Design Loads of Building Structures (GB50009-2012): the maximum crosswind roof accelerations along Y direction are 0.426 m/s^2, 0.381 m/s^2, respectively; the maximum crosswind roof accelerations along X direction are 0.399 m/s^2, 0.308 m/s^2, respectively. However, the threshold of structural

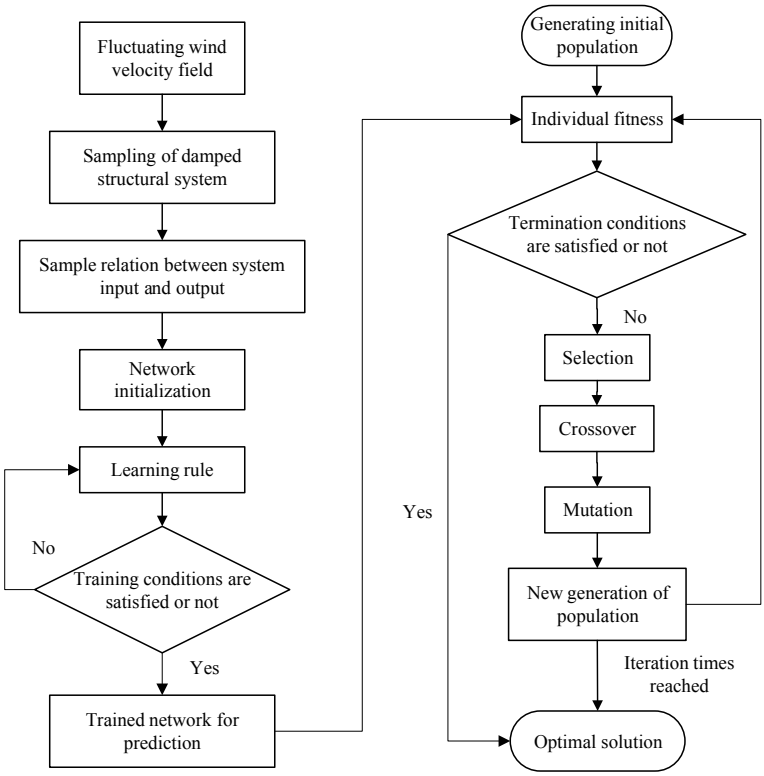

Fig. 7.8 Flowchart of SVM-based genetic algorithm

roof acceleration are defined as 0.28 m/s^2 for public buildings, 0.20 m/s^2 for apartment buildings, respectively, in terms of the Chinese code JGJ99-1998. It is seen that the structural wind-induced roof acceleration surpasses the threshold around 50%. Therefore, considering a successful structural control strategy such that the wind-induced comfortability satisfies with the provisions is a critical task of structural design.

7.4.1 Dimension-Reduced Model of High-Rise Building

The software SAP2000 is employed to perform accurate finite-element modeling as shown in Fig. 7.9. In view of the mass matrix and stiffness matrix derived from the finite-element model, the structural parameters such as the interstory stiffness

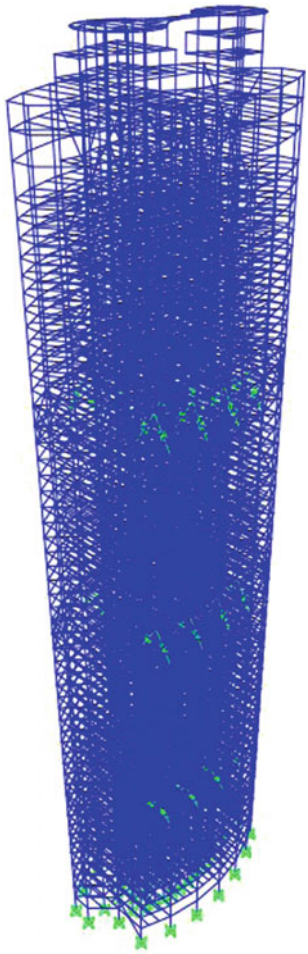

Fig. 7.9 SAP finite-element model of a high-rise building

and story mass of the two-dimensional mass-lumped system can be attained; see Table 7.1. The damping ratio of the first two vibrational modes of the mass-lumped system along X and Y directions are both 0.01. The Rayleigh damping hypothesis, i.e., $\mathbf{C} = a\mathbf{M} + b\mathbf{K}$, is employed in this study. Table 7.2 shows the fundamental periods and the roof acceleration of the finite-element model and of the mass-lumped system. In the comparative study, the basic wind pressure 0.75 kN/m^2 is used.

It is seen that differences of fundamental periods and roof displacements between the simplified mass-lumped system and SAP finite-element model are both in a range of acceptable error. This simplified model underlies the feasibility of stochastic analysis and optimal control of the high-rise building structure.

Table 7.1 Interstory stiffness and story mass of mass-lumped system

Story level	Interstory stiffness along X (10^3 kN/m)	Interstory stiffness along Y (10^3 kN/m)	Story mass (10^3 kg)
1	9400	22,300	1954.6
2	5450	10,700	2478.5
3	4850	8530	2443.3
4	4590	7210	2475.0
5	4560	6800	2493.6
6	6160	8780	2210.8
7	6090	8150	2191.9
8	6030	7400	2192.0
9	6050	6910	2199.4
10	6960	7730	3550.1
11	9420	9120	3052.3
12	6450	6680	2209.4
13	5000	5510	2142.7
14	4620	5040	2143.3
15	4450	4950	2131.2
16	4330	4980	2176.1
17	4240	4660	2143.5
18	4160	4410	2144.3
19	4110	4180	2144.4
20	4040	4070	2151.5
21	4020	4000	2123.4
22	4020	3860	2124.0
23	4090	3700	2124.1
24	4680	3780	3469.2
25	6550	3870	2842.9
26	7560	4420	2949.6
27	4340	3540	2109.0
28	3400	3120	2037.5
29	3150	2930	2037.5
30	3030	2820	2038.5
31	2960	2730	2041.2
32	2910	2670	2040.9
33	2870	2640	2073.4
34	2840	2590	2040.8
35	2800	2500	2017.9
36	2800	2410	2018.3

(continued)

Table 7.1 (continued)

Story level	Interstory stiffness along X (10^3 kN/m)	Interstory stiffness along Y (10^3 kN/m)	Story mass (10^3 kg)
37	2840	2300	1997.1
38	3180	2340	2591.8
39	5080	2710	3429.3
40	4000	2140	3014.0
41	3550	2310	1905.1
42	2720	2030	1938.8
43	2480	1920	1938.9
44	2350	1810	1939.0
45	2260	1750	1954.8
46	2170	1690	1952.1
47	2090	1620	1939.0
48	2010	1550	1938.9
49	1900	1460	1930.5
50	1680	1290	1951.8
51	1560	1180	1934.9
52	1410	1070	1935.6
53	599	514	1731.3
54	742	565	2790.3
55	559	398	1558.8
56	459	301	311.4
57	425	243	325.0
58	330	177	634.5

Table 7.2 Fundamental periods and roof displacements of SAP finite-element model and mass-lumped system

Models	Fundamental period along X direction	Fundamental period along Y direction	Alongwind roof displacement along X direction (m)	Alongwind roof displacement along Y direction (m)
SAP model	4.99	5.26	0.336	0.480
Mass-lumped	4.91	4.94	0.255	0.506
Error (%)[a]	1.6	6.1	5.7	5.4

[a]Error = abs (Mass-lumped system − SAP model)/SAP model

7.4.2 Dynamics Analysis of Model

Using the formulae shown in the Chinese code JGJ99-1998 and in the Chinese code GB50009-2012, the validation of roof acceleration of mass-lumped system subjected to wind load with the occupant-comfortability validation wind pressure 0.45 kN/m^2 is carried out. It is seen from Table 7.3 that using the Newmark-β integral scheme, the dynamic analysis of mass-lumped system gains similar results with the formulae in provisions, and the roof acceleration along Y direction is always larger than that along X direction no matter subjected to alongwind or subjected to crosswind loads. In this study, the alongwind load is simulated by the spatial fluctuating wind velocity model addressed in Sect. 2.5.2. The three basic random parameters included in the wind velocity Fourier spectrum model are valued as: the 10-min mean wind velocity $\bar{U}_{10}$ at the standard height 10 m is assumed to follow the extreme-value type I distribution with mean 26.83 m/s and coefficient of variation 0.1; the surface roughness length z_0 is assumed to follow the log-normal distribution with mean 0.16 m and coefficient of variation 0.2; the zero-phase evolution time T_e is assumed to follow the Gamma distribution with mean 0.902×10^9 s and coefficient of variation 0.1. The crosswind load is simulated by the spectral representation method in conjunction with the experimental crosswind force spectrum and coherence function (Liang et al. 2002). Time histories of representative roof alongwind and crosswind forces of high-rise building are shown in Fig. 7.10. In fact, the building widths along X and Y directions are 37.26 m and 63.34 m, and the aspect ratios are 6.68 and 3.99, respectively. It is indicated that the crosswind effects are of the main concern since the aspect ratios in the two main directions are larger than 3.0 (Liang et al. 2002).

The one-dimensional mass-lumped system along Y direction is investigated, of which the wind-induced vibration and comfortability control are carried out. The circular frequencies of the first ten vibrational modes are denoted by 1.27, 3.15, 4.86, 6.78, 8.20, 10.02, 11.37, 13.23, 14.84, and 17.27 rad/s, respectively.

Table 7.3 Validation of roof acceleration of mass-lumped system subjected to wind load

Cases	Mass-lumped (m/s^2)	PKPM (JGJ99-1998) (m/s^2)	PKPM (GB50009-2002) (m/s^2)
Alongwind along X	0.154	0.080	0.115
Alongwind along Y	0.255	0.132	0.183
Crosswind along X	0.361	0.399	0.308
Crosswind along Y	0.413	0.426	0.381

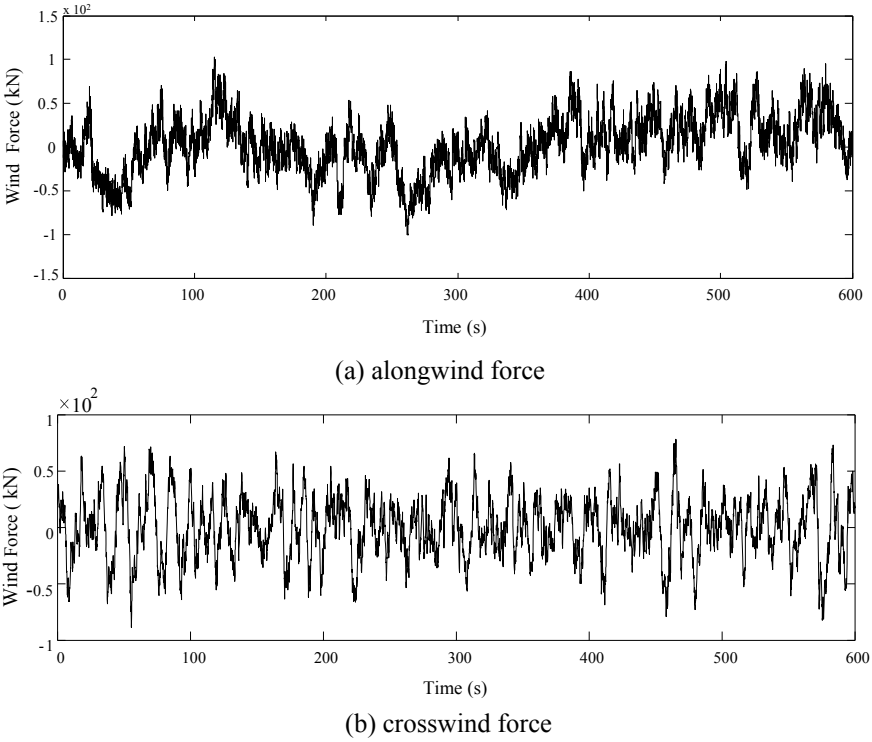

Fig. 7.10 Time histories of representative roof wind forces of a high-rise building

7.4.3 Wind-Induced Comfortability Control

The desired total damping coefficient is first defined through evaluating the structural system with uniformly deployed viscous dampers along story level. It is assumed that the velocity exponents of all the viscous dampers are the same and set as $\alpha = 0.5$. The total damping coefficient is tentatively set as $C_{D,\text{total}} = 8 \times 10^4\,\text{kN(s/m)}^{0.5}$. In this case, the mean of additional damping ratios of the first three vibrational modes is 0.77%, and a comparative result of the roof accelerations with and without viscous dampers is shown in Fig. 7.11. It is seen that with the viscous damper control, the roof acceleration of structure subjected to a representative wind force decreases significantly, of which the maximum acceleration is around 0.21 m/s^2 and reduced to an acceptable range defined by the provisions. Therefore, the total damping coefficient used for the proceeding optimization of parameters and deployments of viscous dampers is set as $C_{D,\text{total}} = 8 \times 10^4\text{kN(s/m)}^{0.5}$.

The parameter and placement optimizations of viscous dampers as both the serviceability criteria SC-1 and SC-2 are carried out. The optimization as the criterion SC-1 employs the genetic algorithm; while the optimization as the criterion SC-

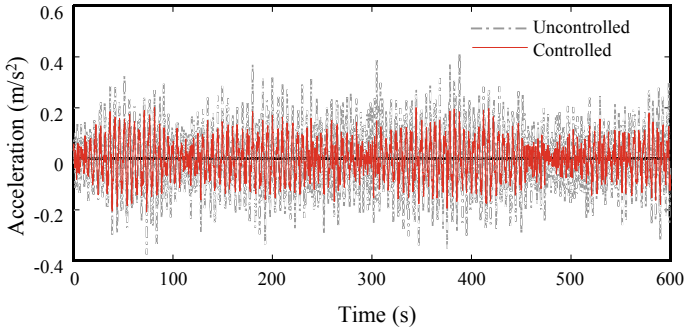

Fig. 7.11 Roof acceleration of structure with and without viscous dampers subjected to representative crosswind force

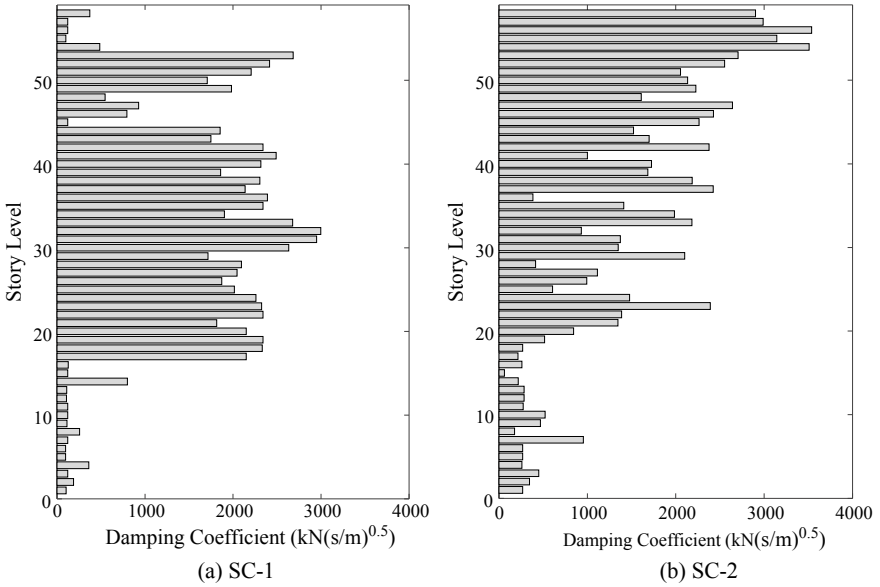

Fig. 7.12 Schematic diagrams of viscous damper deployments as serviceability criteria SC-1 and SC-2

2 employs the SVM-based genetic algorithm. Both optimizations involve a same parameter group of the genetic algorithm: the size of initial population is 1024, the size of other populations is 200, the number of genetic generations is 300, number of variable dimensions is 58, and the parameters k1, k2, k3, k4 for the adaptive crossover and mutation are 0.5, 0.3, 0.7, 0.5, respectively.

With the optimization of the genetic algorithm, the schematic diagrams of viscous damper deployments as the serviceability criteria SC-1 and SC-2 are shown in Fig. 7.12. It is seen that if the traditional criteria on the optimization of mean-

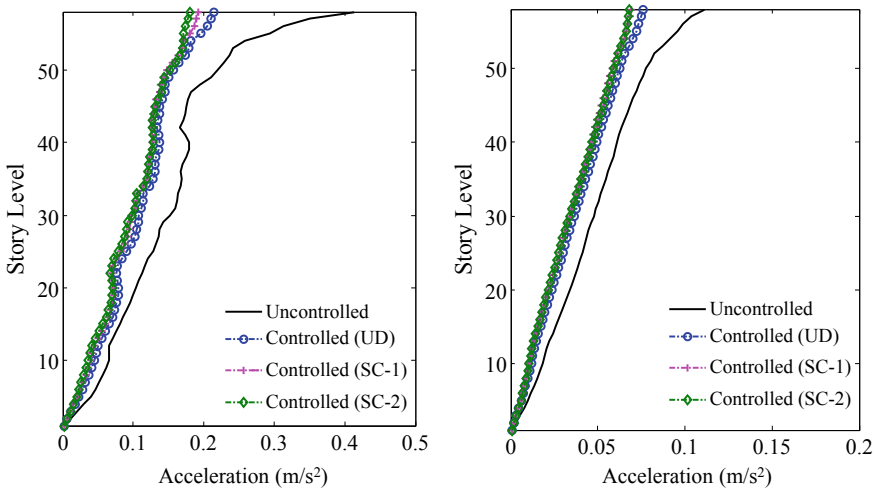

Fig. 7.13 Maximum and standard deviation of story acceleration along story level subjected to representative wind force

square responses such as SC-1 is employed, the middle-level stories; see the stories 17–44 and stories 49–53, need more number of viscous dampers. However, if the exceedance probability based serviceability criteria SC-2 is employed, the high-level stories need more number of viscous dampers, especially at the interstories with a large requirements of viscous dampers such as the stories 50–58.

In order to analyze the control effectiveness of the viscous dampers deployed in the structural system, a comparative study between the wind-induced vibration control by virtue of the optimally deployed viscous dampers as criterion SC-2 and that of the optimally deployed viscous dampers as criterion SC-1 is carried out. Figure 7.13 shows the maximum and standard deviation of story accelerations with and without viscous damper deployments when subjected to a representative wind force. In the figure, the case of viscous dampers uniformly deployed along story level is labeled as Controlled (UD); the cases of optimally deployed viscous dampers as criteria SC-1 and SC-2 are labeled as Controlled (SC-1) and Controlled (SC-2), respectively. All the case calculations resort to the stochastic equivalent linearization method and Newmark-β integral scheme. It is seen that the story accelerations without control are far larger than those with control, which proves the effectiveness of the viscous dampers in the wind-induced comfortability control. One might recognize that the story accelerations of the controlled structure in design as criteria SC-1 and SC-2 are both less than that in the design of uniformly deployed viscous dampers, indicating that the viscous damper deployment as serviceability criteria can gain better control effectiveness, and optimization of viscous dampers exhibits a good trade-off.

Table 7.4 Dynamic reliabilities of roof acceleration of structure subjected to different thresholds

Cases	Thresholds								
	0.2	0.21	0.22	0.23	0.24	0.25	0.26	0.27	0.28
UD	0.0026	0.0177	0.0315	0.0476	0.0814	0.1654	0.6099	0.6855	0.7600
SC-1	0.0057	0.0158	0.0328	0.0490	0.0897	0.4321	0.6497	0.7329	0.7918
SC-2	0.0779	0.1420	0.1999	0.5127	0.7595	0.8269	0.8704	0.9015	0.9326

Units of threshold are (m/s^2)

In fact, the means of the additional former three-order damping ratios of viscously damped structures as the criteria SC-1 and SC-2 are 0.79% and 1.32%, respectively, which are both larger than that of the case with uniformly deployed viscous dampers; i.e., 0.77%. Moreover, the maximum roof accelerations in the cases of optimally deployed viscous dampers as serviceability criteria SC-1 and SC-2 are reduced to 10.6% and 15.7%, respectively, against the case with uniformly deployed viscous dampers. The standard deviations of roof acceleration in the former two cases are reduced to 8.8% and 10.1%, respectively, against the later case. It is well understood that the serviceability criterion using the exceedance probability as the objective argument accommodates better control effectiveness.

The PDF and CDF of equivalent extreme-value roof acceleration can be obtained using the probability density evolution method, as shown in Figs. 7.14 and 7.15. It is seen that the PDF and CDF of uncontrolled roof acceleration incline to the right, and those of controlled roof acceleration as the criteria SC-1 and SC-2 incline to the left to a large extent, by comparison with the case with uniformly deployed viscous dampers. It is also shown that the exceedance probability based serviceability criterion secures better structural habitability. Besides, as shown in Fig. 7.14, the 95% quantile in the case of optimally deployed viscous dampers as criterion SC-2 is much less than those in other two cases. In order to quantitatively assess the differences from the cases, the dynamic reliabilities of roof acceleration subjected to different thresholds are shown in Table 7.4.

It is seen from Figs. 7.14 and 7.15 that the probability density of uncontrolled roof acceleration has a significant difference from those of controlled roof acceleration, which proves again the effectiveness of viscous damper control. In the cases of viscous damper control, the extreme value of roof acceleration as the criterion SC-2 arises to be minimum, then as the criterion SC-1, and the non-optimized case ND has the largest roof acceleration. A straightforward comparison between the case without control and the cases with control can be seen from the 95% quantile. Table 7.4 further shows that in the condition of the same total damping coefficient, the optimal deployment of viscous dampers as the exceedance probability based serviceability criterion can attain the best wind-induced comfortability.

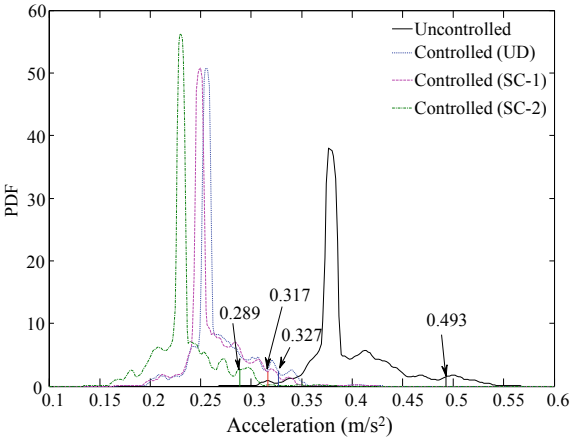

Fig. 7.14 PDFs of equivalent extreme-value roof acceleration and 95% quantiles

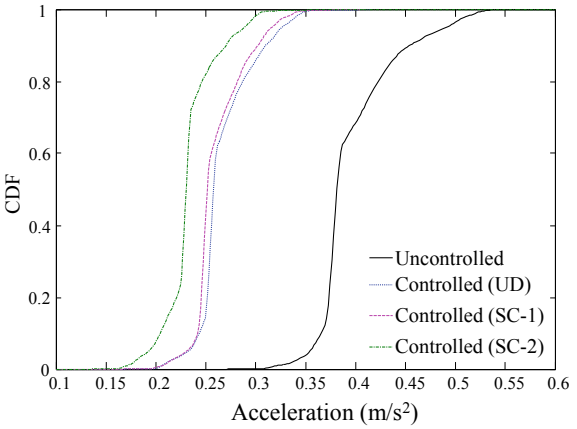

Fig. 7.15 CDFs of equivalent extreme-value roof acceleration

7.5 Discussions and Summaries

The present chapter addresses the stiff ratio of nonlinear structural systems with viscous dampers, in the context of practical challenges on the wind-induced comfortability control of high-rise buildings. The classical equivalent linearization methods including the energy-dissipation equivalent linearization method and the stochastic equivalent linearization technique are investigated. Two families of probabilistic criteria for the optimal design of viscous dampers deployed in the structural system are provided. For validating purposes, the reliability based stochastic optimal control of wind-induced comfortability of a high-rise building in practice is detailed. Some concluding remarks are drawn as follows:

(1) The damper force of nonlinear viscous dampers arises a fast-changing and slow-changing behavior along with the variation of piston velocity, which results in

a stiff problem inherent in the viscously damped structural system. This stiff problem becomes more significant with the increasing of damping coefficient and fundamental period of structures.

(2) Due to the essential nonlinearities inherent in viscously damped structures, the conventional energy-dissipation equivalent linearization method fails to derive an acceptable linearized system. The stochastic equivalent linearization technique is verified to have sufficient accuracy and efficiency in the case of the wind-induced vibration mitigation, which enables the modal superposition method to be used in the highly efficient optimization of nonlinear viscous dampers allocated in high-rise buildings.

(3) The damper allocations as the serviceability criteria of minimum standard deviation and of minimum exceedance probability of roof acceleration have the benefit to reduce the wind-induced vibration significantly, which gain a similar control effectiveness in the case of a same total damping coefficient, and both exhibit a better trade-off than the non-optimized case with uniformly deployed viscous dampers. However, the traditional optimization of viscous damper deployments based on the serviceability criterion of minimum standard deviation of roof acceleration is a deterministic scheme in essence, which has limitation of enhancing the wind-induced comfortability of high-rise building, by comparison with the optimization of viscous damper deployments based on the serviceability criterion of minimum exceedance probability of roof acceleration.

References

Chan CM, Chui JKL (2006) Wind-induced response and serviceability design optimization of tall steel buildings. Eng Struct 28(4):503–513

Chen JB, Zeng XS, Peng YB (2017) Probabilistic analysis of wind-induced vibration mitigation of structures by fluid viscous dampers. J Sound Vib 409:287–305

Chung LL, Wu LY, Yang CSW, Lien KH, Lin MC, Huang HH (2013) Optimal design formulas for viscous tuned mass dampers in wind-excited structures. Struct Control Health Monit 20(3):320–336

Davenport AG (1961) The spectrum of horizontal gustiness near the ground in high winds. Q J R Meteorol Soc 87:194–211

Haykin S (2007) Neural networks: a comprehensive foundation, 3rd edn. Prentice-Hall, Inc

Housner GW, Bergman LA, Caughey TK, Chassiakos AG, Claus RO, Masri SF, Skelton RE, Soong TT, Spencer BF Jr, Yao James TP (1997) Structural control: past, present, and future. ASCE J Eng Mech 123(9):897–971

Huang MF, Chan CM, Kwok KCS (2011) Occupant comfort evaluation and wind-induced serviceability design optimization of tall buildings. Wind Struct 14(6):559–582

Li J, Chen JB (2009) Stochastic dynamics of structures. Wiley, Singapore

Liang SG, Liu S, Li QS, Ming G (2002) Mathematical model of acrosswind dynamic loads on rectangular tall buildings. J Wind Eng Ind Aerod 90(12):1757–1770

Patil VB, Jangid RS (2011) Response of wind-excited benchmark building installed with dampers. Struct Des Tall Spec 20(4):497–514

Peng YB, Ghanem R, Li J (2013) Generalized optimal control policy for stochastic optimal control of structures. Struct Control Health Monit 20(2):187–209
Roberts JB, Spanos PD (1990) Random vibration and statistical linearization. Wiley, West Sussex
Rojas R (1996) Neural networks: a systematic introduction. Springer Science & Business Media
Seleemah AA, Constantinou MC (1997) Investigation of seismic response of buildings with linear and nonlinear fluid viscous dampers. State University of New York at Buffalo, New York
Shampine LF, Reichelt MW (1997) The matlab ode suite. SIAM J Sci Comput 18(1):1–22
Silvestri S, Trombetti T (2007) Physical and numerical approaches for the optimal insertion of seismic viscous dampers in shear-type structures. J Earthq Eng 11(5):787–828
Singh MP, Moreschi LM (2002) Optimal placement of dampers for passive response control. Earthq Eng Struct Dyn 31(4):955–976
Soong TT, Constantinou MC (1994) Passive and active structural vibration control in civil engineering. Springer, New York
Soong TT, Dargush GF (1997) Passive energy dissipation systems in structural engineering. Wiley, New York
Symans MD, Constatinou MC (1998) Passive fluid viscous passive systems for seismic energy dissipation. J Earthq Technol 35(4):185–206
Takewaki I (1997) Optimal damper placement for minimum transfer functions. Earthq Eng Struct Dyn 26(11):1113–1124
Zhang RH, Soong TT (1992) Seismic design of viscoelastic dampers for structural applications. ASCE J Struct Eng 118(5):1375–1391